



# LOFAR Discovery of a Radio Halo in the High-redshift Galaxy Cluster PSZ2 G099.86+58.45

R. Cassano<sup>1</sup>, A. Botteon<sup>1,2,3</sup>, G. Di Gennaro<sup>3</sup>, G. Brunetti<sup>1</sup>, M. Sereno<sup>4,5</sup>, T. W. Shimwell<sup>3,6</sup>, R. J. van Weeren<sup>3</sup>, M. Brüggén<sup>7</sup>, F. Gastaldello<sup>8</sup>, L. Izzo<sup>9</sup>, L. Birzan<sup>7</sup>, A. Bonafede<sup>2,7</sup>, V. Cuciti<sup>7</sup>, F. de Gasperin<sup>7</sup>, H. J. A. Röttgering<sup>3</sup>, M. Hardcastle<sup>10</sup>, A. P. Mechev<sup>3</sup>, and C. Tasse<sup>11,12</sup>

<sup>1</sup> INAF—Istituto di Radioastronomia, via P. Gobetti 101, I-40129 Bologna, Italy; [rcassano@ira.inaf.it](mailto:rcassano@ira.inaf.it)

<sup>2</sup> Dipartimento di Fisica e Astronomia, Università di Bologna, via P. Gobetti 93/2, I-40129 Bologna, Italy

<sup>3</sup> Leiden Observatory, Leiden University, P.O. Box 9513, 2300 RA Leiden, The Netherlands

<sup>4</sup> INAF—Osservatorio di Astrofisica e Scienza dello Spazio, via P. Gobetti 93/3, I-40129 Bologna, Italy

<sup>5</sup> INFN, Sezione di Bologna, viale Berti Pichat 6/2, I-40127 Bologna, Italy

<sup>6</sup> ASTRON—Netherlands Institute for Radio Astronomy, P.O. Box 2, 7990 AA Dwingeloo, The Netherlands

<sup>7</sup> Universität Hamburg, Hamburger Sternwarte, Gojenbergsweg 112, D-21029, Hamburg, Germany

<sup>8</sup> INAF/IASF—Milano, Via A. Corti 12, I-20133 Milan, Italy

<sup>9</sup> Instituto de Astrofísica de Andalucía (IAA-CSIC), Glorieta de la Astronomía s/n, E-18008, Granada, Spain

<sup>10</sup> Centre for Astrophysics Research, School of Physics, Astronomy and Mathematics, University of Hertfordshire, College Lane, Hatfield AL10 9AB, UK

<sup>11</sup> GEPI, Observatoire de Paris, Université PSL, CNRS, 5 Place Jules Janssen, F-92190, Meudon, France

<sup>12</sup> Department of Physics & Electronics, Rhodes University, P.O. Box 94, Grahamstown, 6140, South Africa

Received 2019 June 17; revised 2019 July 17; accepted 2019 July 17; published 2019 August 9

## Abstract

In this Letter, we report the discovery of a radio halo in the high-redshift galaxy cluster PSZ2 G099.86+58.45 ( $z = 0.616$ ) with the LOw Frequency ARray (LOFAR) at 120–168 MHz. This is one of the most distant radio halos discovered so far. The diffuse emission extends over  $\sim 1$  Mpc and has a morphology similar to that of the X-ray emission as revealed by *XMM-Newton* data. The halo is very faint at higher frequencies and is barely detected by follow-up 1–2 GHz Karl G. Jansky Very Large Array observations, which enable us to constrain the radio spectral index to be  $\alpha \lesssim 1.5$ –1.6, i.e., with properties between canonical and ultra-steep spectrum radio halos. Radio halos are currently explained as synchrotron radiation from relativistic electrons that are re-accelerated in the intracluster medium by turbulence driven by energetic mergers. We show that in such a framework radio halos are expected to be relatively common at  $\sim 150$  MHz ( $\sim 30\%$ – $60\%$ ) in clusters with mass and redshift similar to PSZ2 G099.86+58.45; however, at least two-thirds of these radio halos should have a steep spectrum and thus be very faint above  $\sim 1$  GHz frequencies. Furthermore, because the luminosity of radio halos at high redshift depends strongly on the magnetic field strength in the hosting clusters, future LOFAR observations will also provide vital information on the origin and amplification of magnetic fields in galaxy clusters.

**Key words:** galaxies: clusters: individual (PSZ2 G099.86+58.45) – galaxies: clusters: intracluster medium – large-scale structure of universe – radiation mechanisms: non-thermal – X-rays: galaxies: clusters

## 1. Introduction

Cluster-scale ( $\sim$ Mpc-scale), diffuse synchrotron emission is frequently found in high-mass ( $M_{500} \gtrsim 5 \times 10^{14} M_{\odot}$ ) merging galaxy clusters in the form of so-called giant radio halos (RHs), apparently unpolarized emission that fills large cluster volumes (e.g., van Weeren et al. 2019). These sources are characterized by low surface brightnesses and steep spectra ( $\alpha > 1$ , with  $S_{\nu} \propto \nu^{-\alpha}$ ; this is the convention that we adopt here). Their properties and connection with cluster mergers support the idea that they trace turbulent regions in the intracluster medium (ICM) where relativistic particles are trapped and re-accelerated during cluster–cluster mergers (e.g., Brunetti & Jones 2014).

Present statistical studies are limited to relatively low-redshift systems ( $z \lesssim 0.35$ – $0.4$ ; e.g., Venturi et al. 2007, 2008; Cuciti et al. 2015; Kale et al. 2015), with only a handful of halos discovered at  $z \simeq 0.5$ – $0.6$  (Giovannini & Feretti 2000; Bonafede et al. 2009, 2012; van Weeren et al. 2009) and only two at higher redshift: one located in the *El Gordo* galaxy cluster, an exceptionally massive object at  $z = 0.87$  (Lindner et al. 2014), and one in PLCKG147.32–16.59, a cluster at  $z = 0.65$  (van Weeren et al. 2014). At high redshift an increasing fraction of the energy that is dumped into the acceleration of relativistic electrons in RHs is radiated away in

the form of inverse Compton (IC) emission,  $dE/dt \propto (1+z)^4$ . This is expected to cause a decline of the fraction of RHs in high- $z$  galaxy clusters with respect to their low- $z$  counterparts (Cassano et al. 2006). In particular, the fraction of clusters hosting RHs at higher  $z$  is also expected to be very sensitive to the magnetic fields in these systems.

The discovery of high-redshift RHs has been limited by the need for radio observations with high sensitivity to steep spectrum emission and high resolution in order to adequately distinguish the emission from contaminating sources. The advent of the LOw Frequency ARray (LOFAR; van Haarlem et al. 2013), which can produce deep, high-resolution, high-fidelity, low-frequency radio images, has opened up the possibility to study RHs at low frequencies with unprecedented detail and sensitivity (e.g., Shimwell et al. 2016; van Weeren et al. 2016a; Bonafede et al. 2018; Botteon et al. 2018, 2019; Hoang et al. 2018, 2019a, 2019b; Wilber et al. 2018, 2019).

In this Letter, we report on the discovery of a radio halo in the high-redshift galaxy cluster PSZ2 G099.86+58.45 (PSZ2 G099), which was observed as part of the LOFAR Two-meter Sky Survey (LoTSS). LoTSS is an ongoing sensitive  $\sim 100 \mu\text{Jy beam}^{-1}$ , high-resolution,  $\sim 6''$ , 120–168 MHz survey of the entire northern sky (Shimwell et al. 2017, 2019).

PSZ2 G099 is a massive,  $M_{500} = (6.84 \pm 0.48) \times 10^{14} M_{\odot}$ , (Planck Collaboration et al. 2016) and hot,  $kT = 8.9_{-1.1}^{+2.8}$  keV (Sereno et al. 2018), cluster discovered through its Sunyaev–Zel’dovich (SZ) signal by the *Planck* satellite. Recently, the gravitational lensing signal of this cluster has been traced up to 30 Mpc from its center, implying that it sits in a very high-density environment, about six times denser than the average  $\Lambda$ CDM prediction at this redshift (Sereno et al. 2018). The expected complex dynamics around this cluster make the discovery of a RH in this cluster particularly interesting.

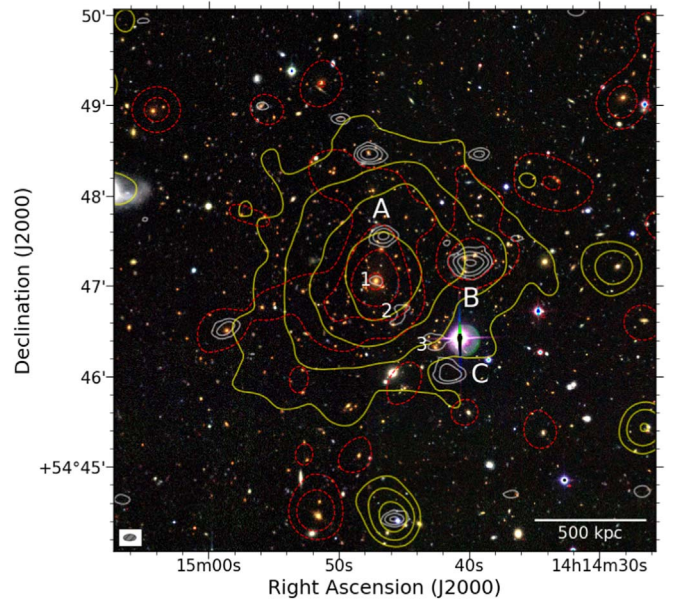
Hereafter, we adopt a  $\Lambda$ CDM cosmology with  $H_0 = 70 \text{ km s}^{-1} \text{ Mpc}^{-1}$ ,  $\Omega_m = 0.3$ , and  $\Omega_{\Lambda} = 0.7$ . With the adopted cosmology,  $1''$  corresponds to a length scale of 6.766 kpc at  $z = 0.616$ .

## 2. Observations and Data Reduction

The LoTSS pointings consist of 8 hr observations in the 120–168 MHz band, which are typically separated by  $\sim 2^{\circ}.6$ . PSZ2 G099 is located at  $\sim 15'$  from the center of pointing P214 +55 (in the region of the HETDEX Spring Field), acquired on 2015 May 14 (ObsID L343224). Data reduction of this pointing was performed with the pipeline described by Shimwell et al. (2019), which performs direction-independent and dependent calibration and imaging of the full LOFAR field of view, using PREFACTOR (van Weeren et al. 2016b; Williams et al. 2016; Mechev et al. 2018; de Gasperin et al. 2019), KILLMS (Tasse 2014a, 2014b; Smirnov & Tasse 2015) and DDFACET (Tasse et al. 2018). To improve the image quality in the direction of PSZ2 G099, we used the products of the pipeline, subtracted all the sources outside a region of  $15' \times 15'$  surrounding the target, and performed extra phase and amplitude self-calibration loops in this sub-field (more details by R. J. van Weeren et al. 2019, in preparation). The LOFAR images shown in this Letter were produced with WSClean v2.6 (Offringa et al. 2014) and have a central frequency of 144 MHz. Uncertainties on the LOFAR integrated flux densities are dominated by errors in the absolute flux scale, which is conservatively set to 20%, in line with LoTSS measurements (Shimwell et al. 2019).

A follow-up observation of PSZ2 G099 was carried out with the Karl G. Jansky Very Large Array (JVLA) in the  $L$ -band (i.e., 1–2 GHz) in C- and D-configurations, for a total time of 4 hr. Following the procedure described by Di Gennaro et al. (2018), we calibrated the antenna delays, bandpass, cross-hand delays, and polarization leakage and angles using the primary calibrators 3C286 and 3C147. The calibration solutions were then applied to the target, and self-calibration on the single data set was performed to refine its amplitude and phase solutions. During the final self-calibration on the combined data set we also employed an additional self-calibration on a bright source located at the edge of the primary beam, whose side lobes affect the cluster radio emission. All the images in this Letter were produced with CASA v5.0 (McMullin et al. 2007) using w-projection (Cornwell et al. 2005, 2008), Briggs weighting with `robust=0`, `nterms=3` (Rau & Cornwell 2011) and are corrected for the primary beam attenuation.

PSZ2 G099 was observed three times with *XMM-Newton* (ObsID: 0693660601, 0693662701, 0723780301) for a total exposure time of 63 ks. Periods of the observations that were affected by soft proton flares are excluded during the analysis by using the Scientific Analysis System tasks. The displayed image is a background-subtracted and exposure-corrected



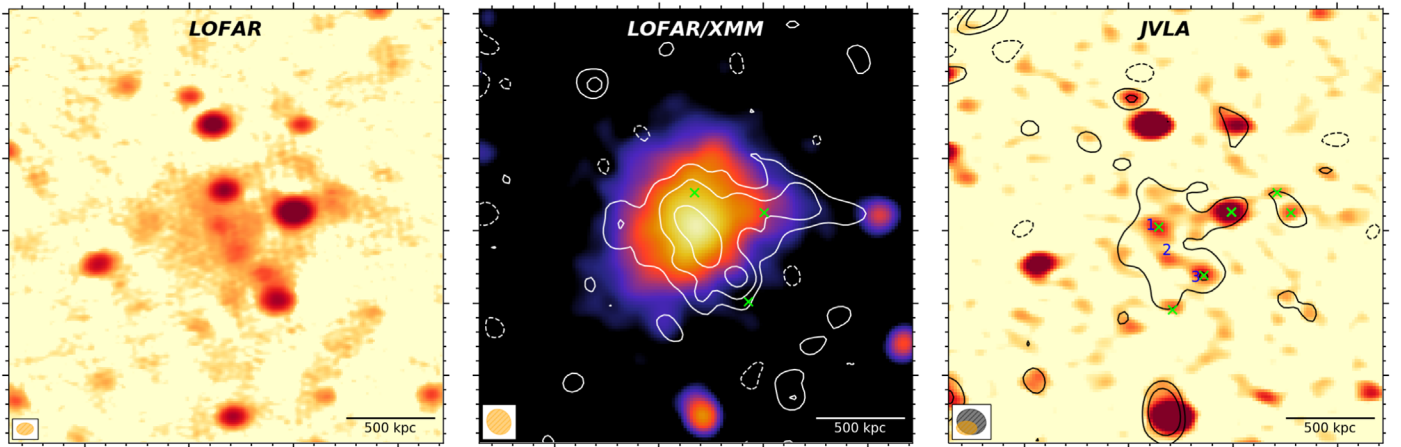
**Figure 1.** CFHTLenS  $g$ -,  $r$ -, and  $i$ -band composite images of PSZ2 G099 with overlaid the LOFAR 144 MHz high-resolution ( $8''3 \times 4''3$ ) contours (white), the *XMM-Newton* contours (yellow), and light density contours of the cluster member galaxies (red dashed). Contours are spaced by a factor of 3 starting from  $5\sigma$  for LOFAR (where  $\sigma = 70 \mu\text{Jy beam}^{-1}$ ) and by a factor of 2 starting from  $5.0 \times 10^{-6} \text{ counts s}^{-1} \text{ pixel}^{-1}$  for *XMM-Newton* (see Figure 2, center). The LOFAR beam is shown in the lower left corner. Labels and numbers show the position of the radio sources (see Section 3 for details).

mosaic image in the 0.5–2.0 keV band of the three ObsIDs where MOS and pn camera images are combined.

## 3. Results

A multi-wavelength view of PSZ2 G099 is reported in Figure 1 where the LOFAR high-resolution contours are overlaid on the Canada–France–Hawaii Telescope Lensing Survey (CFHTLenS; Heymans et al. 2012) image highlighting the presence of the compact radio sources in the direction of the cluster. The X-ray contours from *XMM-Newton* are also reported to show the distribution of the thermal gas. The red contours follow the average surface density of the cluster member galaxies selected in the optical  $i$ -band. We select 3058 galaxies from the CFHTLenS image with photometric redshift within  $\pm 0.06(1 + z_{\text{cl}})$  of the cluster redshift, comparable to the survey photo- $z$  uncertainty. The distribution was smoothed with a Gaussian kernel with a standard deviation of  $50 \text{ kpc } h^{-1}$ . The double-peaked average surface density and the elongated X-ray emission indicate that PSZ2 G099 is in a merging phase.

At medium resolution (Figure 2, left panel), LOFAR clearly reveals extended diffuse emission at the center of the galaxy cluster. Subtracting the emission from point sources and tapering down to  $\sim 20''$  resolution (middle panel) we find a total extent of  $\sim 3 \times 1.5$  in the east–west and north–south direction, respectively, corresponding to a physical extent of  $\sim 1.2 \times 0.6 \text{ Mpc}$ . We classify this emission as an RH due to its extension, morphology, and location in the cluster. The integrated flux density of the sources labeled A, B, and C located in the RH region (Figure 1) is reported in Table 1. Among these only source B is detected in the JVLA image and has a spectral index  $\alpha \simeq 1.5$  (see Figure 2, right panel), meaning that source A and C are very steep spectrum sources ( $\alpha > 1.8$ ). In the high-resolution LOFAR image, another three



**Figure 2.** Left panel: LOFAR 144 MHz medium resolution ( $13''.9 \times 9''.7$ , rms noise  $\sigma = 90 \mu\text{Jy beam}^{-1}$ ). Middle panel: *XMM-Newton* image in the 0.5–2.0 keV band smoothed with a 3 pixel Gaussian kernel (1 pixel =  $2''.5$ ) with low-resolution source-subtracted LOFAR contours ( $21''.6 \times 19''.4$ ,  $\sigma = 200 \mu\text{Jy beam}^{-1}$ ) spaced by a factor of 2 starting from  $2\sigma$ . In both panels,  $-2\sigma$  contours are displayed in dashed lines, while the beam shapes are shown in the bottom-left corners. Right panel: 1–2 GHz high-resolution ( $17''.1 \times 11''.2$ ,  $\sigma = 20 \mu\text{Jy beam}^{-1}$ ) JVLA image with  $2.5\sigma$  and  $5\sigma$  low-resolution source-subtracted JVLA contours ( $24''.5 \times 20''.8$ ,  $\sigma = 36 \mu\text{Jy beam}^{-1}$ ). Numbers in the right panel show the position of the three blobs that are also highlighted in Figure 1.

**Table 1**  
RH Properties

$S_{\text{halo},144 \text{ MHz}}$ (mJy) <sup>a</sup>	$25.3 \pm 5.7$
$S_{\text{halo},1500 \text{ MHz}}$ (mJy)	$\sim 1.5 \pm 0.5$
$P_{\text{halo},1.4 \text{ GHz}}$ ( $10^{24} \text{ W Hz}^{-1}$ ) <sup>b</sup>	$2.85 \pm 0.95$
Halo size (Mpc)	0.6–1.2
144 MHz compact source fluxes (mJy)	$7.0 \pm 1.4$ (A)
	$30.9 \pm 6.2$ (B)
	$7.4 \pm 1.5$ (C)

**Notes.**

<sup>a</sup> Integrated (within  $2\sigma_{\text{rms}}$ ) RH flux density.

<sup>b</sup> Assuming a spectral index of  $\alpha = 1.2$  for the halo emission,  $k$ -corrected.

blobs of emission are detected at  $5\sigma$  (numbered from 1 to 3 in Figure 1), which account for a small total flux density of  $S_{144 \text{ MHz}} \sim 3 \text{ mJy}$ . These are also detected at high frequency, as seen in Figure 2 (right panel).

To disentangle the contribution of the point sources and provide a reliable measurement of the RH flux density, we create an image of diffuse emission only (Figure 2, middle panel) by subtracting the clean components of the sources A, B, and C from the visibilities obtained by applying an inner  $uv$ -cut of  $3.5 \text{ k}\lambda$  (corresponding to a linear size of about 400 kpc at  $z = 0.616$ ) to the data. The flux density of the halo measured within the LOFAR  $2\sigma$  contour is  $S_{144 \text{ MHz}} = 25.3 \pm 5.7 \text{ mJy}$  (this excludes the 3 mJy flux of the three blobs). We verified that the subtraction of the three point sources using  $uv$ -cuts in the range 2.0–5.5  $\text{k}\lambda$  (corresponding to scales of  $\sim 700$ –250 kpc at the cluster redshift) corresponds to variations of the RH flux density of  $\sim 27.2$ –31.6 mJy, which is within the calibration error. The diffuse flux density is  $\sim 15\%$  lower if emission above the  $3\sigma$  level is considered.

In Figure 2 (right panel) we show the JVLA high-resolution ( $17''.1 \times 11''.2$ ) image with the  $2.5\sigma$  contours from the JVLA low-resolution source-subtracted image. The latter image has been obtained after the subtraction of the clean components of the point sources in the field (including those outside the cluster region) using an  $uv$ -cut of  $1.3 \text{ k}\lambda$  (corresponding to  $\sim 500 \text{ kpc}$ ) and  $\text{robust} = -0.5$ , and then tapering at  $\sim 20''$  resolution. The rms noise of this map is  $36 \mu\text{Jy beam}^{-1}$ . Diffuse emission from the RH region is barely detected (the halo is not clearly

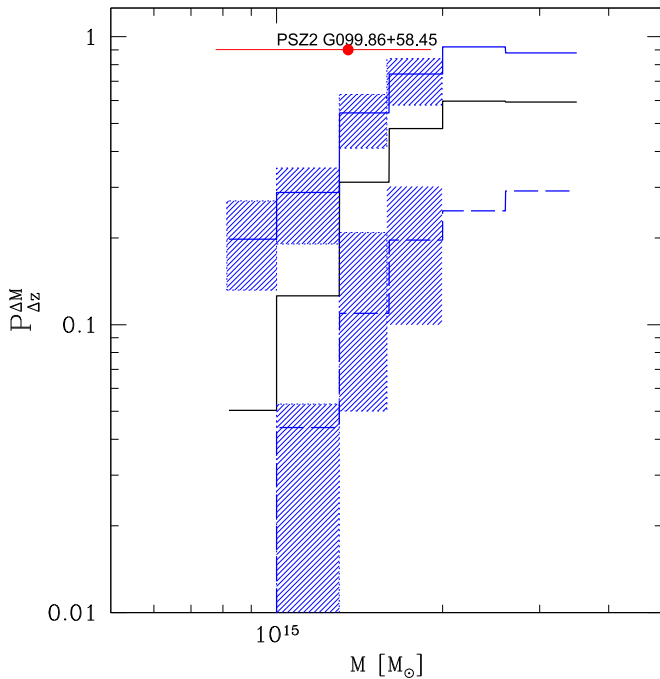
detected at  $3\sigma$ ) but shows some similarity with the RH seen by LOFAR. However, the JVLA image appears to be contaminated by residuals of radio emission by individual sources. Indeed, from the un-tapered map in which point sources have been subtracted, we estimate that a residual contribution of  $\sim 1 \text{ mJy}$  can still be attributed to point sources, which leads to a residual RH flux density of 1.5 mJy within  $2\sigma$ . Because of the very low brightness of the halo we evaluated the statistics of the diffuse flux extracted from similar regions around the RH measuring residual flux densities, which range between  $\approx -0.3 \text{ mJy}$  and  $+0.6 \text{ mJy}$ . This provides an uncertainty in the determination of the RH flux of  $\approx \pm 0.5 \text{ mJy}$  at 1.5 GHz.

#### 4. Discussion

Observing high- $z$  RHs provides unique information about the physics of these sources in an extreme environment. In fact, models for the origin of RHs at such early times are challenged by the strong IC-losses of relativistic electrons ( $dE/dt \propto E^2(1+z)^4$ ), which would compete and hamper the acceleration of high-energy electrons and reduce the synchrotron luminosity that is generated by a factor  $B^2/B_{\text{cmb}}^2$ . Under these conditions the maximum synchrotron frequency emitted by the electrons accelerated in RHs depends on  $B/B_{\text{cmb}}^2$  (Cassano et al. 2006) and thus the magnetic field sets the frequency window where the emission can be observed.

To investigate this point, we derive the formation probability of RHs in a cluster with mass and redshift similar to PSZ2 G099 using the statistical model developed by Cassano & Brunetti (2005; see also Cassano et al. 2006, 2010), which is based on the turbulent re-acceleration scenario. These models match the observed fraction of clusters with RHs derived in mass-selected cluster sample at low- $z$  (Cuciti et al. 2015). In such a framework, the synchrotron spectra of RHs steepen at high frequencies because turbulent re-acceleration is balanced by radiative losses of relativistic electrons. This steepening makes it difficult to detect RHs at frequencies higher than the frequency  $\nu_s$ , at which the steepening becomes severe.<sup>13</sup> As a simplified approach to estimating the occurrence of RHs at a

<sup>13</sup>  $\nu_s$  is defined as the frequency where the synchrotron spectrum is  $\alpha = 1.9$ , with  $\alpha$  calculated between  $\nu_s/2.5$  and  $\nu_s$  (see Cassano et al. 2010, for details).



**Figure 3.** Probability of forming RHs with  $\nu_s \gtrsim 120$  MHz (solid curves) and with  $\nu_s \gtrsim 1400$  MHz (dashed curves) as a function of the cluster virial mass in the redshift range 0.6–0.7, for  $B = 1 \mu\text{G}$  (black curve) and  $B = 4.8 \mu\text{G}$  (blue lines). For the latter case, the  $1\sigma$  uncertainty derived through Monte Carlo calculations is also shown (blue shadowed regions; see the text).

given frequency  $\nu_0$ , we assume that only halos with  $\nu_s > \nu_0$  can be observed at  $\nu_0$ . Massive merging clusters should statistically have larger values of  $\nu_s$ , making them detectable at relatively high frequencies ( $\sim\text{GHz}$ ), while less energetic mergers are expected to produce RHs with lower  $\nu_s$ , which are only detectable at low frequencies ( $< \text{few } 100 \text{ MHz}$ ). The latter are referred to as ultra-steep spectrum RHs (USSRHs<sup>14</sup>) and are predicted to be the dominant class of RHs in low-frequency radio surveys, such as LoTSS (Brunetti et al. 2008; Cassano et al. 2010; Wilber et al. 2018). Theoretically, the two classes of RHs, the canonical and USSRHs, mark the extremes of a continuous distribution of properties of these radio sources.

In Figure 3, we show the probability to form RHs with  $\nu_s \gtrsim 120$  MHz (solid curves) and with  $\nu_s \gtrsim 1400$  MHz (dashed curves) for clusters in the redshift range 0.6–0.7. We assume two values for the average magnetic field strength in the RH region:  $\sim 1 \mu\text{G}$  (black line) and  $B = 4.8 \mu\text{G}$  (blue line). The latter value corresponds to the magnetic field that maximizes the lifetime of relativistic electrons radiating at a given observing frequency at the redshift of the system (i.e.,  $B \simeq B_{\text{cmb}}/\sqrt{3} \simeq 4.8 \mu\text{G}$ ), and thus it should be considered an upper limit for the model expectations. For the case  $B = 4.8 \mu\text{G}$ , we also report the resulting probabilities derived by 1000 Monte Carlo extractions of galaxy cluster samples from the pool of simulated merger trees (shadowed blue regions). Considering the virial mass of PSZ2 G099,  $M_v \simeq (1.35 \pm 0.57) \times 10^{15} M_{\odot}$  (Serenio et al. 2017), we find that at low frequency the probability of forming an RH in such a cluster is at most 40%–60%, and this drops to about 30% when considering  $B \sim 1 \mu\text{G}$ . We conclude that RHs in clusters that are similar to PSZ2 G099 should be fairly common in

LOFAR surveys. On the other hand, the probability of forming RHs in these systems at high frequencies ( $\nu_s \simeq 1400$  MHz) is found to depend critically on the magnetic field in the emitting volume. The maximum probability ( $B = 4.8 \mu\text{G}$ ) is about 20%, whereas a very small probability (below the percent level, not visible in Figure 3) is obtained considering  $B = 1 \mu\text{G}$ . The drop in probability between low and high frequencies is essentially due to the presence of USSRHs that glows up preferentially at lower frequencies.

For the specific case of PSZ2 G099 the spectrum is not measured well; however, our constraint  $\alpha \lesssim 1.5\text{--}1.6$  implies that we can exclude the case of an RH with an extremely steep spectrum, and that the radio properties of PSZ2 G099 could be intermediate between those of canonical and USSRHs. We measure an RH flux density at 1.5 GHz of  $\sim 1.5 \pm 0.5 \text{ mJy}$ , implying a 1.4 GHz radio power ( $k$ -corrected)  $P_{1.4} \simeq (2.85 \pm 0.95) \times 10^{24} \text{ W Hz}^{-1}$ , which is consistent with the  $P_{1.4}\text{--}M_{500}$  correlation observed in intermediate-redshift clusters (Cassano et al. 2013). This provides information on the magnetic field in the RH volume. The expected radio luminosity is  $P_{\text{syn}} \propto \eta_{\text{rel}}(\rho v_i^3/L_{\text{inj}})/(1 + (B_{\text{cmb}}/B)^2)$  (where  $\eta_{\text{rel}}$  accounts for the fraction of turbulence dissipated in particle acceleration). Although the turbulent dissipation rate ( $\rho v_i^3/L_{\text{inj}}$ , where  $\rho$  is gas density,  $v_i$  is turbulent velocity, and  $L_{\text{inj}}$  is the turbulence injection scale) can be larger in dynamically young high- $z$  clusters than in low- $z$  ones, the fact that the radio power of PSZ2 G099 is similar to its lower- $z$  counterparts suggests that  $B$  in this cluster is at least similar to that in low- $z$  ones.

This finding provides important information for models of amplification of  $B$  in galaxy clusters, in particular on the origin of the seed field that is stirred and amplified by turbulence and small-scale dynamo (Dolag et al. 2005; Donnert et al. 2018; Vazza et al. 2018). Because the dynamo mechanism is a slow process that requires several turbulent eddy-turnover times (several Gyr, e.g., Vazza et al. 2018, and references therein) our observations suggest an important role of active galactic nuclei and galactic winds in setting a significant seed field in the ICM at high redshift.

At the same time it should be stressed that PSZ2 G099 is sitting in a special region of the universe, which was found to be about six times denser than the average density of the universe at that redshift (Serenio et al. 2018); therefore, its RH could be unique. The effect of the large-scale environment (environment-bias; see Mao et al. 2018, and references therein) can trigger the formation of an RH: in such a place more merger/accretion episodes are expected to bias the halo growth with respect to a cluster of similar mass in less denser regions of the universe. As a consequence, future analysis of LOFAR surveys will be very important to constrain the formation rate of RHs at high- $z$  and the origin of magnetic fields in these systems.

## 5. Conclusions

We report on the discovery of a  $\sim \text{Mpc}$  (total extent) RH in the PSZ2 G099 cluster using LOFAR observations at 120–168 MHz carried out for the LoTSS. At a redshift of  $\sim 0.616$ , it is among the most distant RHs discovered so far, and the furthest away to have been discovered by LOFAR to date.

The halo is also barely detected by 1–2 GHz follow-up JVLA observations that constrain the radio spectral index to be  $\alpha \lesssim 1.5\text{--}1.6$ , i.e., with properties between canonical and ultra-

<sup>14</sup> RHs with  $\alpha > 1.5$  are considered USSRHs (see the discussion in Brunetti 2004; Brunetti et al. 2008).

steep spectrum radio halos. The estimated 1.4 GHz radio power locates the halo on the observed  $P_{1.4}-M_{500}$  correlation, meaning that the magnetic field strength in this cluster should be not much different from that of other low- to intermediate-redshift halos in clusters with similar mass.

We show that current turbulent re-acceleration models predict that RHs in clusters similar to PSZ2 G099 should be common ( $\sim 30\%$ – $60\%$ ) at low frequencies; however, at least two-thirds of these RHs should be USSRHs and thus be very faint at high frequencies. This shows the power of LOFAR as a unique machine to discover RHs at high- $z$ .










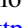


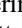


Furthermore, because the fraction of clusters with RHs (and with USSRHs) at high- $z$  and their luminosity depend on the magnetic field in these systems, we claim that LOFAR statistical studies of high- $z$  RHs will provide vital information on the origin of magnetic fields in galaxy clusters.

This Letter is based on data obtained from the International LOFAR Telescope (ILT) under project code LC3\_008. LOFAR (van Haarlem et al. 2013) is the Low Frequency Array designed and constructed by ASTRON. It has observing, data processing, and data storage facilities in several countries, which are owned by various parties (each with their own funding sources), and are collectively operated by the ILT foundation under a joint scientific policy. The ILT resources have benefited from the following recent major funding sources: CNRS-INSU, Observatoire de Paris and Université d’Orléans, France; BMBF, MIWF-NRW, MPG, Germany; Science Foundation Ireland (SFI), Department of Business, Enterprise and Innovation (DBEI), Ireland; NWO, The Netherlands; The Science and Technology Facilities Council, UK; Ministry of Science and Higher Education, Poland; Istituto Nazionale di Astrofisica (INAF), Italy. This research made use of the Dutch national e-infrastructure with support of the SURF Cooperative (e-infra 180169) and the LOFAR e-infra group. The Jülich LOFAR Long Term Archive and the German LOFAR network are both coordinated and operated by the Jülich Supercomputing Centre (JSC), and computing resources on the Supercomputer JUWELS at JSC were provided by the Gauss Centre for Supercomputing e.V. (grant CHTB00) through the John von Neumann Institute for Computing (NIC). This research made use of the University of Hertfordshire high-performance computing facility and the LOFAR-UK computing facility located at the University of Hertfordshire and supported by STFC [ST/P000096/1], and of the LOFAR IT computing infrastructure supported and operated by INAF, and by the Physics Dept. of Turin University (under the agreement with Consorzio Interuniversitario per la Fisica Spaziale) at the C3S Supercomputing Centre, Italy. M.S. acknowledges financial contribution from ASI-INAF n.2017-14-H.O. The Leiden LOFAR team acknowledge support from the European Research Council under the FP/2007-2013/ERC Advanced Grant NEWCLUSTERS-321271. R.J.v.W. acknowledges support from the VIDIL research program, project number 639.042.729, which is financed by the NWO. A.B. acknowledges financial support from the ERC-Stg DRANOEL, no 714245, and from the MIUR grant FARE SMS. L.I. acknowledges support from funding associated with Juan de la Cierva Incorporacion fellowship IJCI-2016-30940. A.P.M. acknowledge support from the NWO/DOME/IBM program “Big Bang Big Data: Innovating ICT as a Driver For Astronomy,” project

#628.002.001. G.B. acknowledges partial support from ASI/INAF n. 2017-14-H.O.

Facilities: LOFAR, XMM-Newton, JVLA.

### ORCID iDs

R. Cassano  <https://orcid.org/0000-0003-4046-0637>  
 A. Botteon  <https://orcid.org/0000-0002-9325-1567>  
 G. Di Gennaro  <https://orcid.org/0000-0002-8648-8507>  
 G. Brunetti  <https://orcid.org/0000-0003-4195-8613>  
 M. Sereno  <https://orcid.org/0000-0003-0302-0325>  
 T. W. Shimwell  <https://orcid.org/0000-0001-5648-9069>  
 R. J. van Weeren  <https://orcid.org/0000-0002-0587-1660>  
 M. Brüggén  <https://orcid.org/0000-0002-3369-7735>  
 F. Gastaldello  <https://orcid.org/0000-0002-9112-0184>  
 L. Izzo  <https://orcid.org/0000-0001-9695-8472>  
 A. Bonafede  <https://orcid.org/0000-0002-5068-4581>  
 F. de Gasperin  <https://orcid.org/0000-0003-4439-2627>  
 H. J. A. Röttgering  <https://orcid.org/0000-0001-8887-2257>  
 M. Hardcastle  <https://orcid.org/0000-0003-4223-1117>  
 A. P. Mechev  <https://orcid.org/0000-0002-8950-8999>

### References

- Bonafede, A., Brüggén, M., Rafferty, D., et al. 2018, *MNRAS*, 478, 2927  
 Bonafede, A., Brüggén, M., van Weeren, R., et al. 2012, *MNRAS*, 426, 40  
 Bonafede, A., Feretti, L., Giovannini, G., et al. 2009, *A&A*, 503, 707  
 Botteon, A., Shimwell, T. W., Bonafede, A., et al. 2018, *MNRAS*, 478, 885  
 Botteon, A., Shimwell, T. W., Bonafede, A., et al. 2019, *A&A*, 622, A19  
 Brunetti, G. 2004, *JKAS*, 37, 493  
 Brunetti, G., Giacintucci, S., Cassano, R., et al. 2008, *Natur*, 455, 944  
 Brunetti, G., & Jones, T. W. 2014, *IJMPD*, 23, 1430007  
 Cassano, R., & Brunetti, G. 2005, *MNRAS*, 357, 1313  
 Cassano, R., Brunetti, G., Norris, R. P., et al. 2012, *A&A*, 548, A100  
 Cassano, R., Brunetti, G., Röttgering, H. J. A., & Brüggén, M. 2010, *A&A*, 509, A68  
 Cassano, R., Brunetti, G., & Setti, G. 2006, *MNRAS*, 369, 1577  
 Cassano, R., Etori, S., Brunetti, G., et al. 2013, *ApJ*, 777, 141  
 Cornwell, T. J., Golap, K., & Bhatnagar, S. 2008, *ISTSP*, 2, 647  
 Cornwell, T. J., Golap, K., & Bhatnagar, S. 2005, in ASP Conf. Ser. 347, *Astronomical Data Analysis Software and Systems XIV*, ed. P. Shopbell, M. Britton, & R. Ebert (San Francisco, CA: ASP), 86  
 Cuciti, V., Cassano, R., Brunetti, G., et al. 2015, *A&A*, 580, A97  
 de Gasperin, F., Dijkema, T. J., Drabant, A., et al. 2019, *A&A*, 622, A5  
 Di Gennaro, G., van Weeren, R. J., Hoefl, M., et al. 2018, *ApJ*, 865, 24  
 Dolag, K., Grasso, D., Springel, V., & Tkachev, I. 2005, *JCAP*, 1, 009  
 Donnert, J., Vazza, F., Brüggén, M., & ZuHone, J. 2018, *SSRV*, 214, 122  
 Giovannini, G., & Feretti, L. 2000, *NewA*, 5, 335  
 Heymans, C., Van Waerbeke, L., Miller, L., et al. 2012, *MNRAS*, 427, 146  
 Hoang, D. N., Shimwell, T. W., van Weeren, R. J., et al. 2018, *MNRAS*, 478, 2218  
 Hoang, D. N., Shimwell, T. W., van Weeren, R. J., et al. 2019a, *A&A*, 622, A20  
 Hoang, D. N., Shimwell, T. W., van Weeren, R. J., et al. 2019b, *A&A*, 622, A21  
 Kale, R., Venturi, T., Giacintucci, S., et al. 2015, *A&A*, 579, A92  
 Lindner, R. R., Baker, A. J., Hughes, J. P., et al. 2014, *ApJ*, 786, 49  
 Mao, Y.-Y., Zentner, A. R., & Wechsler, R. H. 2018, *MNRAS*, 474, 5143  
 McMullin, J. P., Waters, B., Schiebel, D., Young, W., & Golap, K. 2007, in ASP Conf. Ser. 376, *Astronomical Data Analysis Software and Systems XVI*, ed. R. A. Shaw, F. Hill, & D. J. Bell (San Francisco, CA: ASP), 127  
 Mechev, A. P., Plaat, A., Oonk, J. B. R., Intema, H. T., & Röttgering, H. J. A. 2018, *A&C*, 24, 117  
 Offringa, A. R., McKinley, B., Hurley-Walker, N., et al. 2014, *MNRAS*, 444, 606  
 Planck Collaboration, Ade, P. A. R., Aghanim, N., et al. 2016, *A&A*, 594, A27  
 Rau, U., & Cornwell, T. J. 2011, *A&A*, 532, A71  
 Sereno, M., Covone, G., Izzo, L., et al. 2017, *MNRAS*, 472, 1946  
 Sereno, M., Giocoli, C., Izzo, L., et al. 2018, *NatAs*, 2, 744  
 Shimwell, T. W., Luckin, J., Brüggén, M., et al. 2016, *MNRAS*, 459, 277  
 Shimwell, T. W., Röttgering, H. J. A., Best, P. N., et al. 2017, *A&A*, 598, A104

- Shimwell, T. W., Tasse, C., Hardcastle, M. J., et al. 2019, *A&A*, **622**, A1
- Smirnov, O. M., & Tasse, C. 2015, *MNRAS*, **449**, 2668
- Tasse, C. 2014a, *A&A*, **566**, A127
- Tasse, C. 2014b, arXiv:1410.8706
- Tasse, C., Hugo, B., Mirmont, M., et al. 2018, *A&A*, **611**, A87
- van Haarlem, M. P., Wise, M. W., Gunst, A. W., et al. 2013, *A&A*, **556**, A2
- van Weeren, R. J., Brunetti, G., Brügger, M., et al. 2016a, *ApJ*, **818**, 204
- van Weeren, R. J., de Gasperin, F., Akamatsu, H., et al. 2019, *SSRv*, **215**, 16
- van Weeren, R. J., Intema, H. T., Lal, D. V., et al. 2014, *ApJL*, **781**, L32
- van Weeren, R. J., Röttgering, H. J. A., Brügger, M., & Cohen, A. 2009, *A&A*, **505**, 991
- van Weeren, R. J., Williams, W. L., Hardcastle, M. J., et al. 2016b, *ApJS*, **223**, 2
- Vazza, F., Brunetti, G., Brügger, M., & Bonafede, A. 2018, *MNRAS*, **474**, 1672
- Venturi, T., Giacintucci, S., Brunetti, G., et al. 2007, *A&A*, **463**, 937
- Venturi, T., Giacintucci, S., Dallacasa, D., et al. 2008, *A&A*, **484**, 327
- Wilber, A., Brügger, M., Bonafede, A., et al. 2018, *MNRAS*, **473**, 3536
- Wilber, A., Brügger, M., Bonafede, A., et al. 2019, *A&A*, **622**, A25
- Williams, W. L., van Weeren, R. J., Röttgering, H. J. A., et al. 2016, *MNRAS*, **460**, 2385